**Crustal-scale fault systems in the Korean Peninsula unraveled by reflection seismic data**

Samuel Zappalá[1], Alireza Malehmir[1], Tae-Kyung Hong[2], Christopher Juhlin[1], Junhyung Lee[2], Myrto Papadopoulou[1], Bojan Brodic[1], Seongjun Park[2], Dongchan Chung[2], Byeongwoo Kim[2], & Jeongin Lee[2]

[1]Dept. of Earth Sciences, Uppsala University, Villavägen 16, Uppsala, Sweden

[2]Dept. of Earth System Sciences, Yonsei University, 50 Yonsei-ro Seodaemun-gu, Seoul, South Korea

*Correspondence to*: Samuel Zappalá (samuel.zappala@geo.uu.se); Tae-Kyung Hong (tkhong@yonsei.ac.kr)

**Key points**

- Reflection seismic imaging of fault systems in Seoul metropolitan area.
- Suggested dependency of the regional seismicity from Chugaryeong fault system.
- Deep geometry reconstruction of three regional fault systems.

**Abstract.** An approximately 40-km long high-resolution reflection seismic profile (P3) was acquired in the metropolitan area of Seoul in South Korea for the purpose of fault system imaging in a highly noisy and challenging urban environment. Two 12t seismic vibrators (mini-vibs) were used as the seismic source. Data were recorded using a dual element seismic spread; 20 m spaced 421 wireless seismic recorders connected to 10 Hz geophones and 20 micro-electro-mechanical (MEMS-based) landstreamer sensors (2 m sensor spacing) attached to one of the vibrators. The purpose of the dual spread employed was to delineate both near-surface and deep structures. The processing results show good quality and the processing work was complemented by different analysis to further constraints the geological interpretation. The survey results provide evidence for the 3D geometry of three fault systems, including Chugaryeong, Pocheon and Wangsukcheon faults. A gently westerly-dipping set of reflectivity underlying a domed-shaped package of reflectivity is interpreted as a fault, and could project to the known surface position of the Pocheon fault. The domed-shaped reflectivity is interpreted as folded and faulted dyke or sill systems. Downward continuation of the interpreted fault intersects the sub-vertical Chugaryeong fault in a zone where the current seismicity is observed, suggesting that these two major fault systems may have jointly evolved in the form of splay faults. Reflections from the Wangsukcheon fault are also present in the data and interpreted to dip approximately 60 degrees to the east, in an opposite direction to the two other faults.

**Plain language summary**

An approximately 40-km long high-resolution reflection seismic profile was acquired in the metropolitan area of Seoul in South Korea for the purpose of in-

depth fault system imaging in a highly noisy and challenging urban environment. Two different types of receivers were used simultaneously to achieve good results from both shallow and deep structures. Processing results have good quality and are complemented with different analysis to further constraints the geological interpretation. The survey results provide evidence for the 3D geometry of three fault systems, including Chugaryeong, Pocheon and Wangsukcheon faults. A gently westerly-dipping structure underlying a domed-shaped structure is interpreted as a fault, and could project to the known surface position of the Pocheon fault. A domed-shaped reflectivity is interpreted as folded and faulted dyke or sill systems. Downward continuation of the interpreted fault intersects the sub-vertical Chugaryeong fault in a zone where the current seismicity is observed, suggesting that these two major fault systems may be connected and jointly evolved. Results from the Wangsukcheon fault are also present in the data and it is interpreted to approximately dip 60 degrees to the east, in an opposite direction to the two other faults.

**Keywords**

Land Seismic Reflection – Hardrock – Megacities – Faults Imaging – Korean Peninsula - Seismicity

# 1 Introduction

The Korean peninsula is an important tectonic link between eastern China and the Japanese islands (Figure 1). Comprised mainly of deformed basement rocks (granitic intrusions and volcanic rocks, and high-grade gneiss and schist, ranging in age from 1.1 to 2.7 Ga), the Korean crust has experienced a long deformation history. The peninsula has until recently been in a stable intraplate seismic state, although major earthquakes are known from historical recordings (hard copies and drawings), occurring both on the southern part and close to metropolitan Seoul (Lee and Yang, 2006; Park et al., 2020). After the 2011 Tohoku-Oki mega-thrust Mw 9.0 earthquake in Japan, several plus Mw 5.0 earthquakes have been recorded in the peninsula. The 2011 mega-thrust perturbed the Korean crust resulting in coseismic displacements of ~2-4 cm around the east and west coasts of the peninsula and is likely responsible for the subsequent increased seismic activity in the country (Hong et al., 2017). In 2016, the largest event, the Gyeongju Mw 5.4 earthquake (ML 5.8), recorded in the recent history of modern seismic monitoring in South Korea occurred.

Metropolitan Seoul is densely populated and is home to over 20 million inhabitants; a strong earthquake in the city can be devastating. For preparedness and public safety purposes, it is essential to investigate potentially active fault systems, their structures, geometries and triggering mechanisms. This can help to estimate potential damages, magnitudes and places where reinforcements are necessary for infrastructure and housing (Singh et al.,1980; Rosenblueth et al.,1990; Wells et al., 1994). The need to investigate subsurface structures

below major cities is a common problem since many mega-cities are in high geo-hazard risk regions. However, these environments are typically noisy (both electric/electromagnetic and ambient seismic noise) and with logistical challenges, making many geophysical investigations difficult to impossible. Nonetheless, different methods have been attempted, including drilling as one example (Zoback et al., 2013). Geophysical methods, especially seismic ones, can be a method of choice although ambient vibrational noise and ground-receiver coupling are major challenges in mega-cities (Sato et al., 2009; Malehmir et al., 2011; Ishiyama et al., 2016). Despite these problems, different studies show that adopting solutions specifically developed for high-resolution imaging in urban settings can bring important results via high-quality imaging of the subsurface structures, also helping to delineate fault systems at depth that may be important for understanding geo-hazards and for preparedness purposes (Sato et al., 2009; Brodic et al., 2015; Ishiyama et al., 2016; Malehmir et al., 2015, 2016, 2017, 2022).

To evaluate the feasibility, and develop specific strategies, for high-resolution seismic imaging of geo-hazards in mega-cities, two novel active-source reflection seismic profiles (P1 and P2) were acquired in November 2020 in the central and wider metropolitan area of Seoul in South Korea. The survey aimed at showing a spatial relationship between the Chugaryeong fault system (one of the crustal-scale fault systems crossing the entire peninsula and active until the Quaternary) and the recorded seismicity in the last 10 years (Hong et al., 2018 and 2021). Recent studies suggest that the Chugaryeong fault is near-vertical and still active showing a dominant strike-slip mechanism from focal mechanism solutions (Hong et al., 2018, 2021). The Pocheon and Wangsukcheon faults, mapped east of the Chugaryeong fault, appear to form splay faults as they approach each other in the city (Figure 1). Other smaller faults are also expected between these three major crustal fault systems although with poor or no surface exposures. P1 was located on the northern side of metropolitan Seoul while P2 was positioned in the central part of the city where the Chugaryeong fault intersects a cluster of seismicity. Given the encouraging results from the 2020 survey, especially along P1 where reflections down to 8-9 km depth were imaged and showed both spatial and temporal correlation with the clustered seismicity (Malehmir et al., 2022), a new survey was justified to shed light on the overall subsurface geometry of the three major fault systems. In July 2021, a new seismic profile (P3), approximately 40 km, was acquired (Figure 1). It was positioned between P1 and P2 on the northern outskirts of metropolitan Seoul where it was logistically possible to acquire the new profile. P3 intersects all the three major fault systems, Chugaryeong, Pocheon and Wangsukcheon, and marks the longest single profile ever recorded in South Korea. The main goals of this study are (1) establish a depth relationship of the three major faults for the first time, (2) reconstruct fault geometries and intersections and (3) investigate correlation between reflections and the recorded seismicity in the region. We demonstrate that the new profile allows 3D positioning of these fault systems and speculate on a fault-bend fold structure suggesting a reverse

movement component along it. Some of the recorded seismicity may also occur at the intersection of the Chugaryeong fault with other major faults.

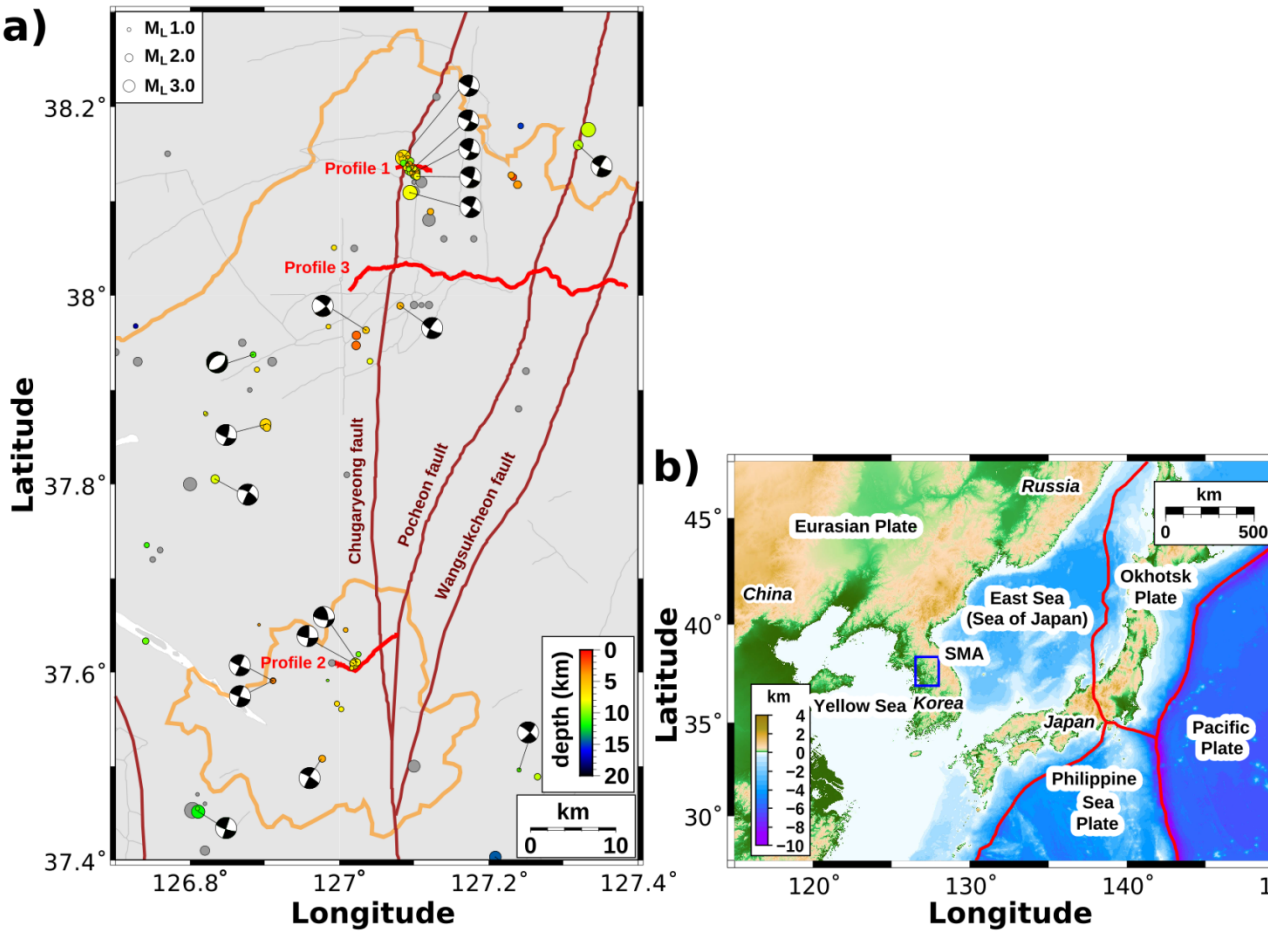


**Figure 1.** (a) Recent seismicity recorded in South Korea and the location of the seismic profile (P3, acquired in July 2021) in relation to the previous ones (P1 and P2) acquired in November 2020 (Malehmir et al., 2022). Profile P3 crosses the three major fault systems with the aim to reconstruct their geometries at depth. The locations of the fault systems are approximate and based on extrapolation from rivers and valleys. (b) Major plate boundaries surrounding the study area.

## 2 Seismicity and geology of the Korean peninsula

The Korean peninsula can generally be characterized by three major Paleoproterozoic massifs (lithotectonic domains), Nangrim, Gyeonggi, and Yongnam, separated by the Imjingang and Ogcheon belts (Chough et al., 2000). The new reflection seismic profile P3 was acquired on the northwestern margin of the Gyeonggi massif crossing different lithologies and the previously discussed faults.

The Gyeonggi massif in the central part of the peninsula is comprised of granitic, gneissic and basaltic rocks. Geological units range from Paleoproterozoic to Cretaceous except for the basalts and fluvial deposits that are of Quaternary age. These rocks are crosscut by major fault systems from Paleozoic to Quaternary (Choi et al., 2012; Bae and Lee, 2016). The most represented lithologies are granite, gneiss and schist, with also the occurrence of basalts, metasediments and dykes. The area shows evidences of four main deformation phases. The first one is related to N-S compression in Late Permian-Early Triassic, followed by a N-S extensional phase in Middle-Late Triassic that resulted in ductile shear and normal faulting. In Middle-Late Jurassic a NNW-SSE compression caused NW-dipping thrust systems. The last phase is characterized by N-S to NNE-SSW right strike-slip faults associated with NNW-SSE folds and to the formation of different Cretaceous basins. The three fault systems (Figure 2) that are the focus of this seismic survey are related to the last deformation phase, which show evidence of activity during the Quaternary and that are possibly still active (KIGAM, 2008). Recent studies show the occurrence of seismic clusters close to the main faults, especially to the Chugaryeong fault, suggesting that they are in some way controlled by the current stress field (Hong et al., 2021). During the last decades, several projects have studied these faults, working on their ages, kinematics and geometries, using trenches when possible (i.e., Han and Lee, 2019 and references therein). Results of these studies suggest high dipping angles for all the faults with the Chugaryeong fault considered to be sub-vertical, Pocheon WNW dipping and Wangsukcheon ESE dipping (Han and Lee, 2019). The main limitation for these studies is the poor exposure of these faults on the surface. Therefore, most of the mapped faults are reconstructed following lithological boundaries and morphological valleys, with real information limited only to small areas. The entire area is geothermally active, as can be seen by the occurrence of different natural hot springs in the area (Lee et al., 2010).

## 3 Seismic data acquisition

Data acquisition along P3 was carried out from the second half of July to the beginning of August 2021 and took approximately 25 days, including line setup, recording and downloading data from wireless recorders (data harvesting). The length of the profile and the environmental factors required active updating of the profile geometry during the acquisition to reach an optimal setup configuration for fold and offset coverage (Figure 2).

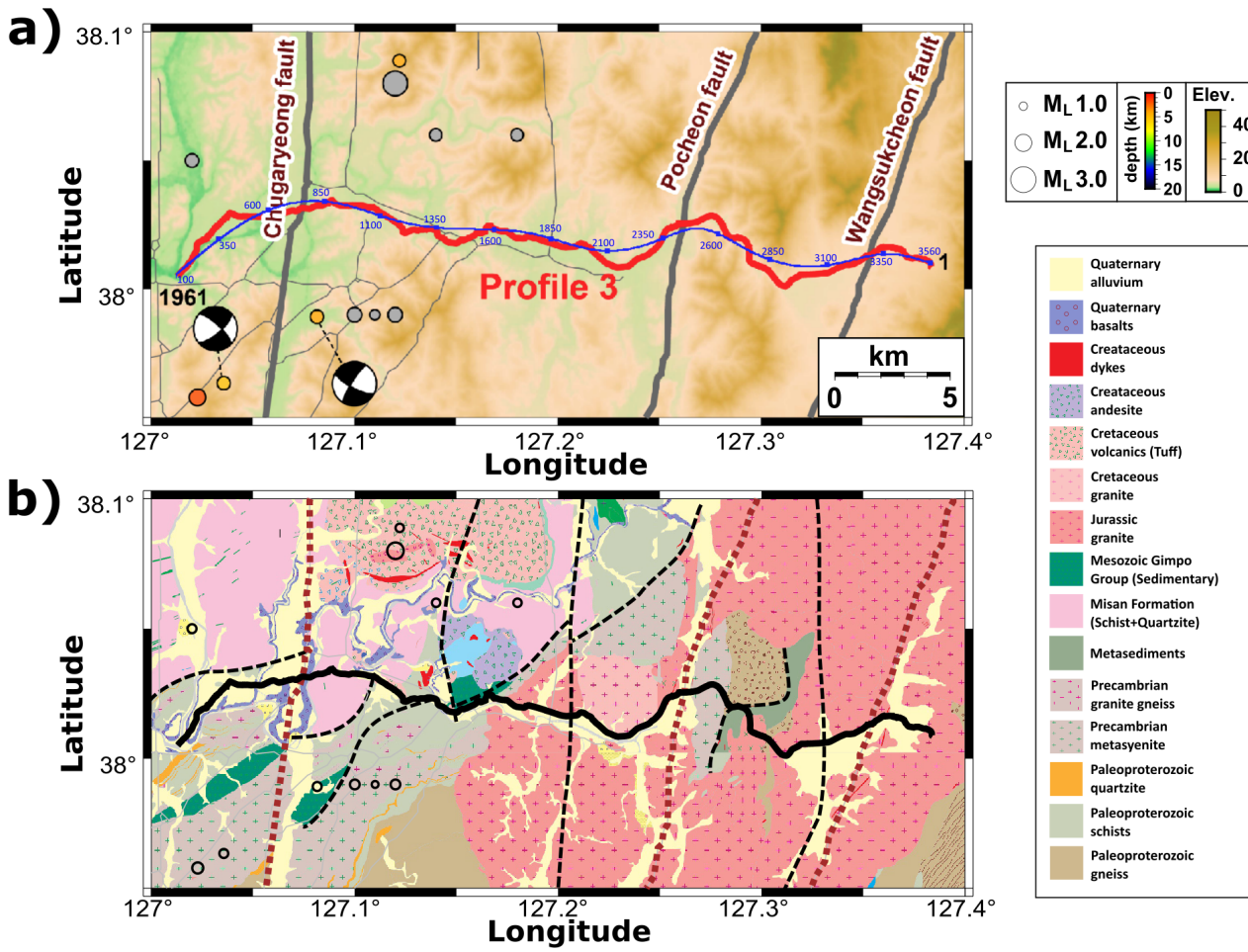


**Figure 2. (a) Seismic profile P3 shown in red with a total length of approximately 40 km was acquired in summer 2021. In blue the common midpoint (CMP) line used to process the data. (b) Geological map of the study area; dashed lines are mapped faults close to the profile. Seismicity of the area is also shown. Grey circles have no focal depth solutions.**

Along the entire profile length, a dual-element seismic spread consisting of wireless seismic recorders connected to 10 Hz vertical geophones and a micro-electromechanical MEMs-based landstreamer was used to acquire the data with the aim of imaging both near-surface and deeper structures. This setup was also used during the acquisition of profiles P1 and P2 (Malehmir et al., 2022). The wireless recorders (total of 421) were used in an asymmetric split-spread roll-along acquisition geometry to cover the entire profile length, with an active spread of 7.4 km. To provide a regular fold and offset coverage, and plan receiver

deployment, different scenarios were evaluated for in what order the receivers should be picked up. Twenty landstreamer mounted MEMS-based recorders (2 m sensor spacing) were towed behind one of the two seismic vibrators used as a seismic source for the survey. The streamer data provided active quality control and GPS time stamping of shot records. The two seismic vibrators (Innova 9t Mini-vibs - UV2) were equipped with an additional weight of 3000 kg to improve ground coupling and operated in a clock-phase synchronized mode to avoid distortion and anti-phase vibration. At every source point, the vibrators (each approximately 7 m long) were positioned with the actual shot position assigned in between the two vibrators, collocated with wireless receivers. Sweeps at both vibrators were simultaneously initiated with initiation of recording of the streamer data and we treat the excited seismic energy as a single source point. To improve the S/N ratio, four sweeps per shot location were generated with the sweep parameters.

With 1961 wireless recorder positions, 17546 landstreamer recorder positions and a receiver spacing of 20 m and 2 m respectively, approximately 40 km of high-resolution seismic data were acquired. The nominal shot spacing achieved was 20 m with a total of 1887 positions. Due to a technical problem, landstreamer recorders were not used during one day of the acquisition, hence they contain only 1736 shot positions. A GPS antenna was used for time-tagging and sampling of the landstreamer data. The time stamps were later used to harvest the corresponding data from the wireless recorders that were autonomously recording during the acquisition. Details of the survey parameters and the acquisition strategy used can be found in Table 1. All wireless receiver positions were accurately surveyed using a cm accuracy DGPS system.

**Table 1. Main seismic data acquisition parameters, Seoul Metropolitan area, July 2021.**

| **Spread parameters** | **Profile 3** |
|---|---|
| **Recording system** | Sercel Lite$^{TM}$ |
| **Survey geometry** | asymmetric split spread, roll-along |
| **No. of receivers** | Wireless: 421 (1-1961 locations)<br>Streamer: 20 (17,546 locations) |
| **No. of shots** | (at 1887 shot points, 4 sweep records/point in most places) |
| **Nominal shot/receiver spacing** | m |
| **Maximum offset** | ~ 7290 m |
| **Source type** | Two 12t, Mini-vibs, 10-140 Hz linear, 18 s long, peak force of 95 kN per vibrator |
| **Geophone** | Wireless: vertical 10 Hz, spike<br>Streamer: three component (3C) MEMs, only vertical used for analysis |
| **Sampling interval** | ms |

| Spread parameters | Profile 3 |
|---|---|
| **Record length** | s (15 s after cross-correlation) |
| **Wireless data downloading** | Based on landstreamer GPS-time tagging |
| **Total no. of traces** | Wireless: 701,020<br>Streamer: 34,435 |
| **Maximum CMP fold** | Wireless: 382<br>Streamer: 97 |
| **Geodetic surveying** | DGPS corrected where needed using national elevation grid data |

Before starting the acquisition, different sweep parameters were tested. Tests were carried out at receiver location 10 (easternmost part of the profile) with 40 landstreamer recorders deployed for this purpose. Given the earlier successful study of a similar setup (Malehmir et al., 2022), the intention was primarily to check if the two sources were phase-locked and synchronized. Different linear upsweeps with frequency ranges 5-120 Hz, 5-140 Hz, 10-120 Hz and 10-140 Hz, with varying lengths of 16 and 18 s were tested. Theoretical sweeps were used for the cross-correlation. After studying the corresponding shot records, 10 Hz was chosen as the starting frequency, to avoid excessive surface-wave energy excited by the source, and 140 Hz as the ending one. An 18 s sweep length was chosen to make sure enough time was given to allow buildup of both low and high frequencies.

# 4 Seismic data analysis

## 4.1 Reflection data processing

The overall quality of the data is reasonable given the high noise level background in the region, with a CMP fold coverage between 180-220 and a maximum offset of ca. 7 km. The highest quality data were registered on the eastern and in the central part of the profile with numerous shot and receiver gathers exhibiting clear reflectivity and first breaks up to maximum offsets (Figure 3). The western parts of the profile show noisier data due to line position close to a big city and major roads. Generally, reflections are more continuous on some receiver gathers, showing that geophone-ground coupling in the city environment is key to acquiring quality data. For this reason, when possible, processing steps were carried out on receiver gathers. An interesting phenomenon of this dataset is the strong presence of back-scattering of surface-waves in some parts of the profile (Figure 4). Given their clear locations, they are used in this study to complement the interpretation of imaging results.

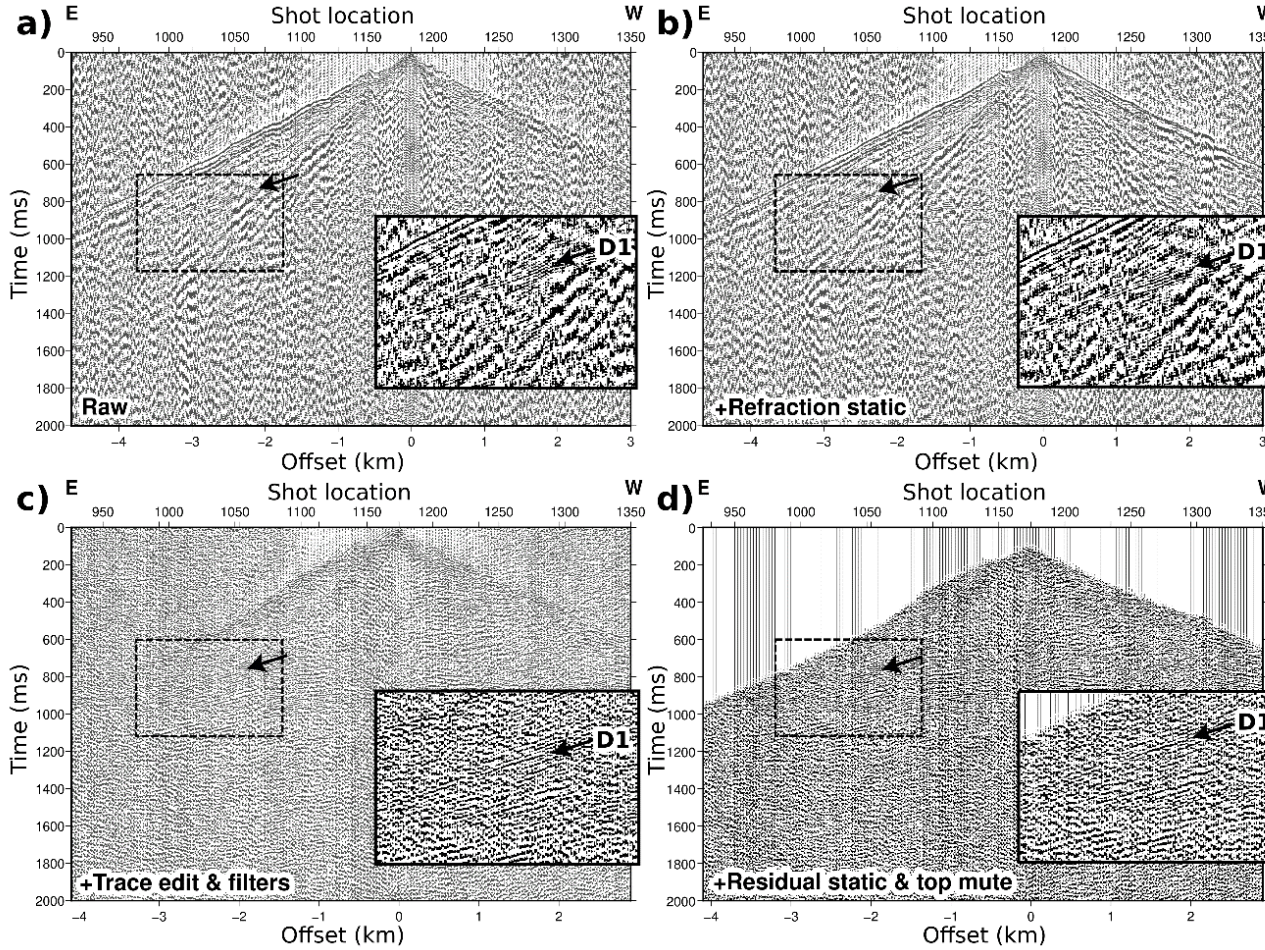


**Figure 3.** (a) An example of raw receiver gather at station 1185, in the central part of the profile. Clear first breaks up to 5 km offsets and a series of reflections (D1) are visible. (b-d) The same receiver gather as (a) but after different processing stages, (b) after the application of refraction static corrections, (c) after spectral equalization, deconvolution, time variant filter and median filter, and (d) after surface-consistent residual static corrections and top mute. Note how the reflections marked by black arrows become more continuous and stronger after each of these steps.

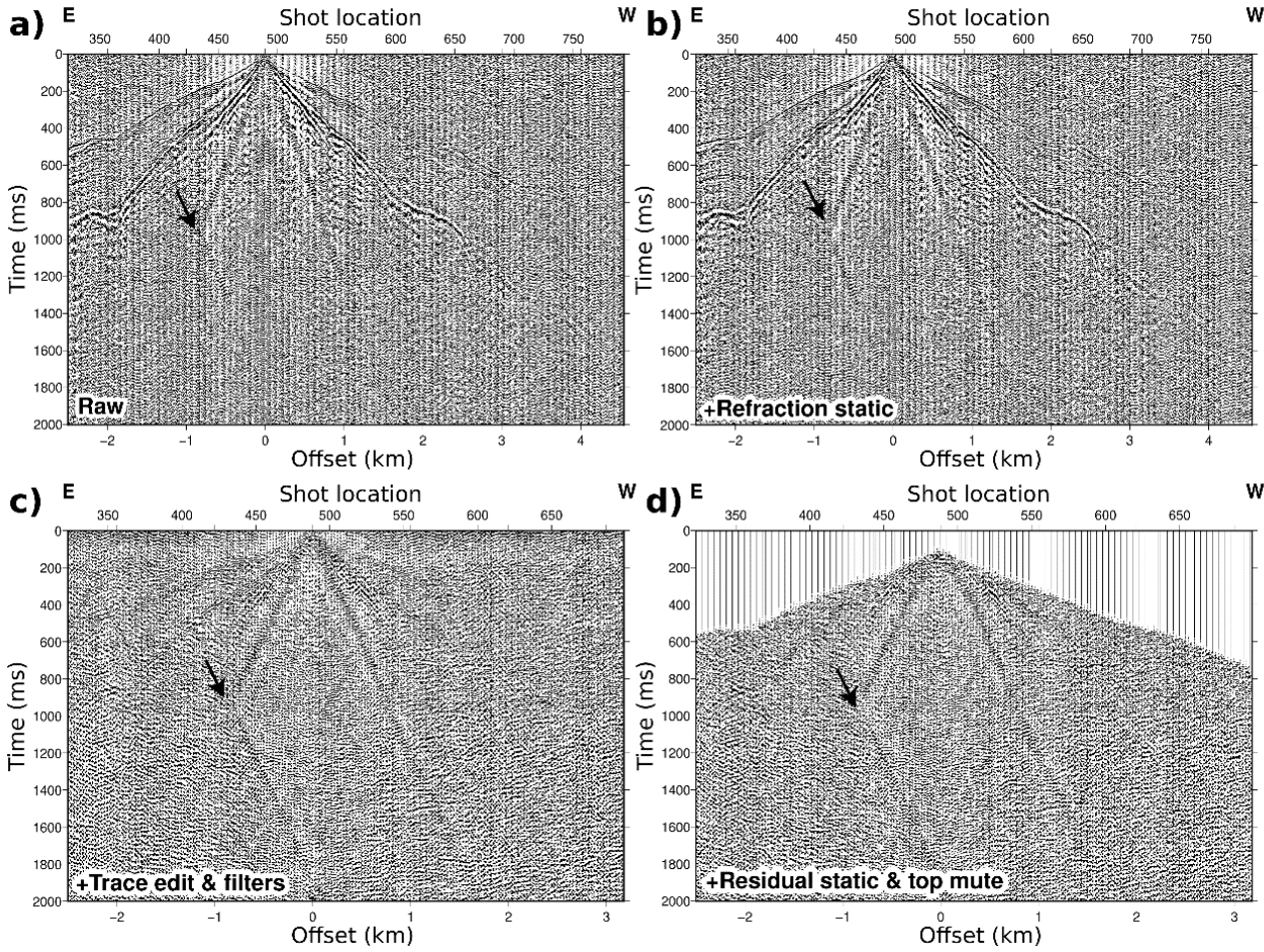


**Figure 4. (a) An example of raw receiver gather at station 487 showing notable backscattering of surface-waves marked by black arrows. (b-d) The same receiver gather as (a) but after different processing stages, (b) after the application of refraction static corrections, (c) after spectral equalization, deconvolution, time variant filter and median filter, and (d) after surface-consistent residual static corrections and top mute.**

Landstreamer and wireless data were processed separately and merged after stack using a similar procedure as described by Malehmir et al. (2022). Landstreamer data were handled with a straightforward processing scheme with the aim of imaging the top of the bedrock. The streamer processing is largely based on building a velocity model for the NMO corrections and maintaining higher frequencies. In contrast, the wireless recorder data processing required carefully selected processing steps and parameters due to deeper targets and a lower S/N

ratio.

Four seconds of wireless recorder data were processed. First-break picking was the most time-consuming step, however rewarding as the refraction static correction step was crucial for improved imaging. Other important steps were trace editing, median filters, and velocity analysis coupled with surface-consistent residual static corrections. For stacking purposes, a slalom CMP line was positioned following the centers of midpoint distributions; an identical CMP geometry was also used for the landstreamer data to enable merging of the two data sets. After stack, phase-shift migration was applied and data were time-to-depth converted using a constant velocity of 6000 m/s. Table 2 shows the key reflection seismic processing steps applied to the data.

**Table 2. Key reflection processing steps.**

| **Steps** | **Profile 3** |
|---|---|
| **1** | Read SEGD data |
| **2** | Zero-time corrections and cross-correlation with the theoretical sweep |
| **3** | Vertical stacking (4 repeated sweep records) |
| **4** | Geometry setup (CMP spacing 10 m for both streamer and wireless data) |
| **5** | First-break picking |
| **6** | Trace edit |
| **7** | Surface-consistent refraction static corrections |
| **8** | Elevation static corrections (200 m, 5000 m/s) |
| **9** | Notch filter: 60 Hz |
| **10** | Predictive deconvolution (150 ms window and 24 ms gap) |
| **11** | Spectral balancing: 10-30-90-110 Hz |
| **12** | Band-pass filter: 10-25-110-130 Hz (time variant) |
| **13** | Median filters (2500 m/s, 5000 m/s) |
| **14** | AGC (300 ms) |
| **15** | Velocity analysis (constant velocity stacks - CVS) |
| **16** | Local crossdip correction |
| **17** | Surface-consistent residual static corrections (2 runs) |
| **18** | NMO corrections (40% stretch mute) |
| **19** | Stack (diversity) |
| **20** | FX-deconvolution |
| **21** | Balance amplitude |
| **22** | Migration (phase shift, 5000-6500 m/s) |
| **23** | Time-to-depth conversion (constant velocity, 6000 m/s) |
| **24** | Export for plotting and 3D visualizations |

### 4.2 First-break traveltime tomography

A first-break traveltime tomography model was computed using the picked first breaks for the refraction static corrections using a diving-wave finite-difference based code (Trygvasson et al., 2002). Although the code calculates ray paths and traveltimes in 3D space, the model was forced to be 2D by taking a large cell size perpendicular to the profile. The starting model was set to take into consideration the topography. After considering the characteristics of the picked first-breaks and some tests with different starting models, a model that uses 1000 m/s below the topography with a velocity gradient reaching 5500 m/s at 100 m depth was chosen. A 10 m by 10 m cell size in inline and depth directions were adopted for the computation. After 8 iterations the resulting RMS value was 4.011 ms.

## 5 Results and interpretation

The unmigrated stacked section obtained from the landstreamer data (Figure 5a) is focused on the bedrock reflection. The reflection can be mapped in high resolution and has good lateral continuity. Some areas, especially on the western side of the profile where the main city is located, show a less clear bedrock reflection. The weathering layer thickness appears to be less than 50 m, with the top of the bedrock at most places close to the surface. The bedrock mostly shows a rough surface morphology characterized by steps that could represent fault displacements or partial erosional surfaces (Figure 5a). As the bedrock reflection is relatively shallow there was no attempt to migrate these data (Black et al., 1994).

The first-break traveltime tomography of the wireless data and the landstreamer reflection results show good correspondences, suggesting a good correspondence between the two processing methods. The tomography results show a good-quality image along the whole profile, also close to the main city as the short offsets are better picked than at far offsets on the wireless recorders. As for the landstreamer section, the weathering layer (with a velocity of about 1300 m/s) has a thickness that goes from 10 to 50 m. The bedrock shows a rough surface with clear steps also in the tomography results (Figure 5b).

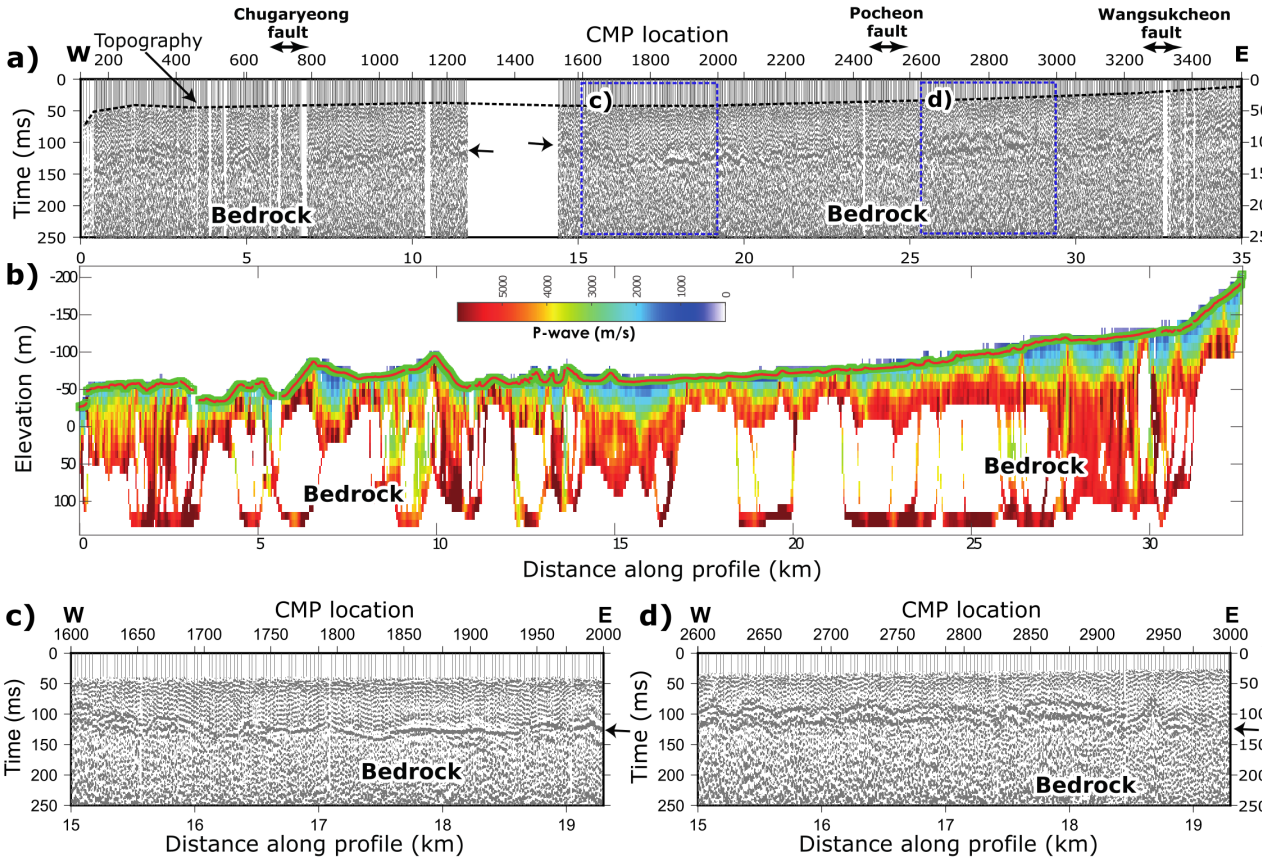


**Figure 5. (a) Unmigrated stacked section of the MEMs-based landstreamer data. Arrows point at the interpreted bedrock reflection. (b) First-break traveltime tomography results obtained from the wireless recorder data. Note the correspondence between the low-velocity structures and bedrock reflection geometries. (c-d) Highlighted part of the landstreamer stacked section (a) shown for better display and quality assurance purposes.**

Results from the wireless data are focused on deeper reflection imaging since they cover larger offsets and are better designed for this purpose. An unmigrated stacked section of the profile is shown in Figure 6. The most reflective part (D1) is in the central area of the profile, between CMP 1200 and 2000, where a strong package of reflectivity (also clearly observable on some receiver gathers, e.g., Figure 3) from 0.7 to 1.2 s with a domed shape pattern is visible. This main reflection on its eastern bottom intersects a west-dipping package of reflections, but with albeit lower continuity (F2). They project to the surface at the location of the Pocheon fault, where also a strong back-scattering of surface-waves is observed. This interpretation needs to be viewed with caution as the projection

downwards and to the surface may not necessarily be valid. An important feature of the data is the strong reflectivity observed in the central part of the profile (D1). While the nature of this strong reflective zone is unclear, the presence of mafic dykes and natural geothermal fields, suggesting fluid presence that can enhance the reflectivity, in the area (Lee et al., 2010) make them a plausible explanation for the origin of the reflectivity. If the interpretation of the geometry is correct and if there is any fault underlying this domed-shaped reflective zone, then there might be a relationship between the geometry of the domed-shaped reflective zone and an underlying fault.

The apparent bending of the reflective zone (D1) towards the underlying planar-type reflectivity may imply a sense of movement or shearing with a "fault-bend fold" pattern (Figure 7), suggesting that much of the movement along the planar surface (fault) is then reverse (Suppe and Medwedeff, 1990). In this interpretation scenario, the reflective package D1 should be from materials that are isolated and planar in nature like sills and dykes, which is highly likely as they are present on the geological map of the area. There might also be fluids in this area as geothermal fields are known in the central region of the profile (Lee et al., 2010).

On the most eastern part of the profile, an east-dipping reflection (F1) is visible from 0.2 to 0.6 s; however, it is not strong and can only be observed in a portion of the shot/receiver gathers (Figure 6). The reflection projects to the location of the Wangsukcheon fault (Figure 2). Therefore, it is likely generated by the Wangsukcheon fault plane, implying a zone of brittle structures.

On the western part of the profile, various sub-horizontal reflections with a low lateral continuity are visible down to 2.5 s (or approximately 7.5 km depth). Between CMP 700 and 800, no coherent reflection is observed, and strong noise is present. This region coincides with the Chugaryeong fault; hence the lack of reflectivity may be explained by the sub-vertical nature of this fault (F3). The strong surface-wave back scattering energy observed at this location further supports this interpretation. Vertical barriers like faults are natural features that can back-scatter surface-waves (Blonk and Herman, 1994; Yu et al, 2014).

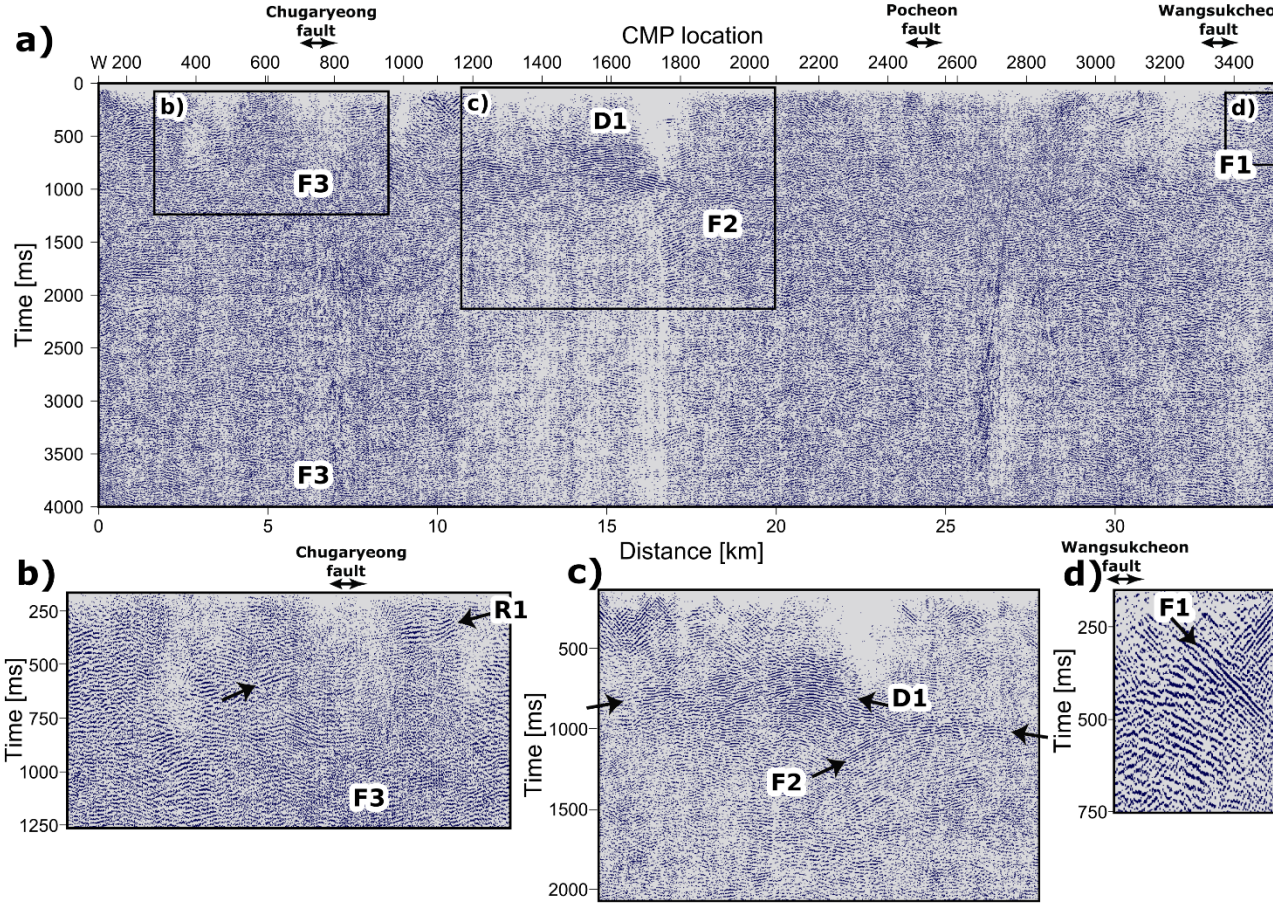


**Figure 6.** (a) Unmigrated stacked section of the wireless recorder data. For display purpose, three zoomed windows are shown in (b-d) where a transparent channel of reflectivity is interpreted to represent the Chugaryeong fault (F3); the domed reflective package (D1) with underlying reflections (F2), in the central part of the profile, may represent the Pocheon fault position, a crossdip correction of 10 degree to the north has been applied; an east-dipping reflection interpreted to be from the Wangsukcheon fault (F1).

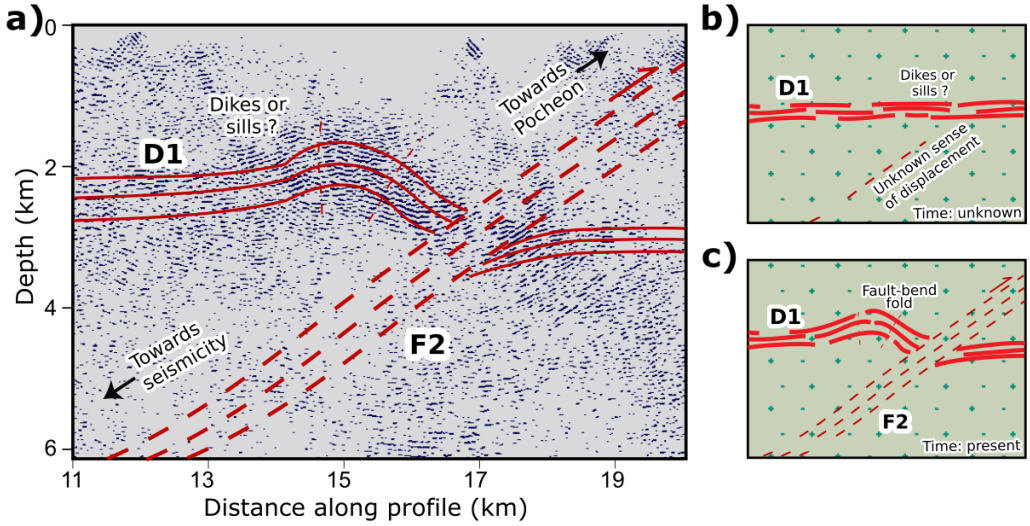


**Figure 7. (a) A portion of the migrated stacked section of P3 illustrating a possible fault-bend-fold structure from D1 caused by F2 faulting (likely a thrust system). Sketch showing the structures (b) before and (c) after faulting.**

# 6 Discussion

## 6.1 3D reflection traveltime modeling

To justify some of the seismic interpretations, we scrutinized the data further. For the most eastern reflection (F1), because it comes near the surface and it is clearly observed in several shot and receiver gathers, we were able to model the reflection traveltime response based on Ayarza et al. (2000), assuming a similar strike as the Wangsukcheon fault, a velocity above the fault of 5000 m/s, and the position where the reflection intersects the surface. A strike of N20E and dip of 60E can explain the reflection traveltime observed in the real data, hence further supporting its origin as being from the Wangsukcheon fault.

## 6.2 Origin of strong surface-waves back scatterings

Given the strong surface waves back-scattering observed in the data (i.e., Figure 4), it was important to further analyze their properties. The Zerwer et al. (2005) method, as implemented for multifold data by Colombero et al. (2018), was applied to estimate the location of sharp lateral variations in the subsurface and the corresponding maximum affected wavelength. This method shows interesting results for locating lateral variations at different places along the profile. These locations were compared with the bedrock reflection from the landstreamer data and tomography results from the wireless recorders (Figure

5), as well as shot and receiver gathers where surface-waves are clearly back scattered. Two of these surface-wave back scattering sources are particularly strong: (1) where the Chugaryeong fault is mapped and (2) at CMP location 2840. Although no corresponding faults are represented in the geology at CMP 2840, a sharp geological contact between Paleoproterozoic gneiss and Jurassic granite suggests the presence of some tectonic structure that could be the reason for the surface-wave back-scattering energy. The two locations show, respectively, a minimum frequency of 12 Hz and 17 Hz with a maximum affected wavelength of 110 m and 100 m. This distinguishes the scattering to be geological in nature and not due to human constructions such as road and bridge foundations. Similar strong back scattered surface waves are also visible at Pocheon fault surface location, but showing a lower intensity.

## 6.3 Crossdip analysis and out-of-plane structures

The crooked nature of the profile implies that the trace midpoints are distributed along a 3D zone, allowing evaluation of out-of-the-plane structures and apparent dips for several reflections. This effect was further exploited using a crossdip analysis approach (Bellefleur et al., 1995; Nedimović and West, 2003; Malehmir et al., 2006, 2009; Rodriguez-Tablante et al., 2007; Beckel and Juhlin, 2019). For the reflection (F2) underlying the domed-shaped reflections (Figures 6c and 7), we were able to estimate a crossdip angle of 10 degrees to the north and a true dip of approximately 30 degrees towards NW. The crossdip analysis could only be achieved thanks to the midpoint coverage provided by the crookedness of the profile.

## 6.4 Fault 3D geometries and seismicity

The information gained from all the analyses were compiled and used to construct 3D surfaces of potential major fault systems along the profile (Figure 8). Based on these surfaces, it is possible to interpret the location and geometry of two of the major fault systems in the area, namely the Wangsukcheon (F1) and Chugaryeong (F3) faults with high reliability. The Wangsukcheon fault dips opposite to what was first expected, especially if considering that it would be a splay fault from the Chugaryeong fault. This implies that the Wangsukcheon fault is likely a separate and unrelated fault system with respect to the two other ones or that it makes a sharp turn as it extends to the northern part of the country (Figure 1). Recent excavation works (Han and Lee, 2019) and historical studies (Kim, 1973) further support our interpretation of the dip direction of the Wangsukcheon fault and the reliability of the 3D reflection traveltime modeling work. The Chugaryeong fault is not imaged as a reflection, as expected for a sub-vertical feature that has also been argued from focal mechanism solutions (Hong et al., 2018, 2021). Nonetheless, there are related features that support the sub-vertical nature of the Chugaryeong fault such as (i) the absence of coherent reflection, (ii) the sharp and important lateral variation visible at the bedrock level in both the landstreamer data and tomography and (iii)

the extremely high surface wave back-scattered energy. All these features are observed at the fault surface expression (Choi et al., 2012). The reflections (F2) underlying the domed reflectivity package (Figures 6c and 7) have a true dip of approximately 30 degrees towards the NW. This dip angle was to a certain degree speculated upon by Malehmir et al. (2022) for Pocheon fault but is different from previous suggestions (Hong et al., 2021). Surface projection of these reflections corresponds to the location of strong surface-wave back scattered energy at the mapped position of the Pocheon fault. Interestingly, projecting the reflections towards depth results in them intersecting with the recorded seismicity, suggesting an intersection with the Chugaryeong fault. While this is highly speculative, a possible scenario might be that the Pocheon fault is a splay fault from the Chugaryeong fault system and that the recorded seismicity occurs at their intersection. Malehmir et al. (2022) argued for the same geometry, however they had a much shorter profile, hence their arguments were more speculative. Another possible scenario will be that the F2 reflection is generated by a different fault that becomes steeper close to the surface. Pocheon fault instead will be subvertical, as suggested from seismological focal mechanism inversion studies (Hong et al, 2021), hence not imaged. There may be a third scenario explaining the NW-dipping package of reflectivity underlying the domed-shape reflectivity (F2), namely dykes as they are also interpreted to be present in the domed-shape reflectivity and diffractivity.

Given the curved-shaped nature of the reflectivity overlying these planar sets of reflections, we argue for a thrust (reverse mechanism) fault system associated with these reflections. Thrust faults are known to generate fault-bend folds and this implies the dome-shaped reflectivity might be the result of a growth fault system that was active sometimes (even until now). In this scenario, the reflective package would initially have consisted of sill-type intrusions, which were then folded, and likely also faulted, forming the dome-shaped reflectivity observed in the central part of the study area (Figure 7). Assuming this interpretation scenario is correct, a direct implication is that both the Chugaryeong and F2 faults might be active. Given the opposite dip direction of the Wangsukcheon, it is likely that any seismicity along this fault should be separately looked at, although the fault appears to be inactive in terms of seismicity recorded in the area.

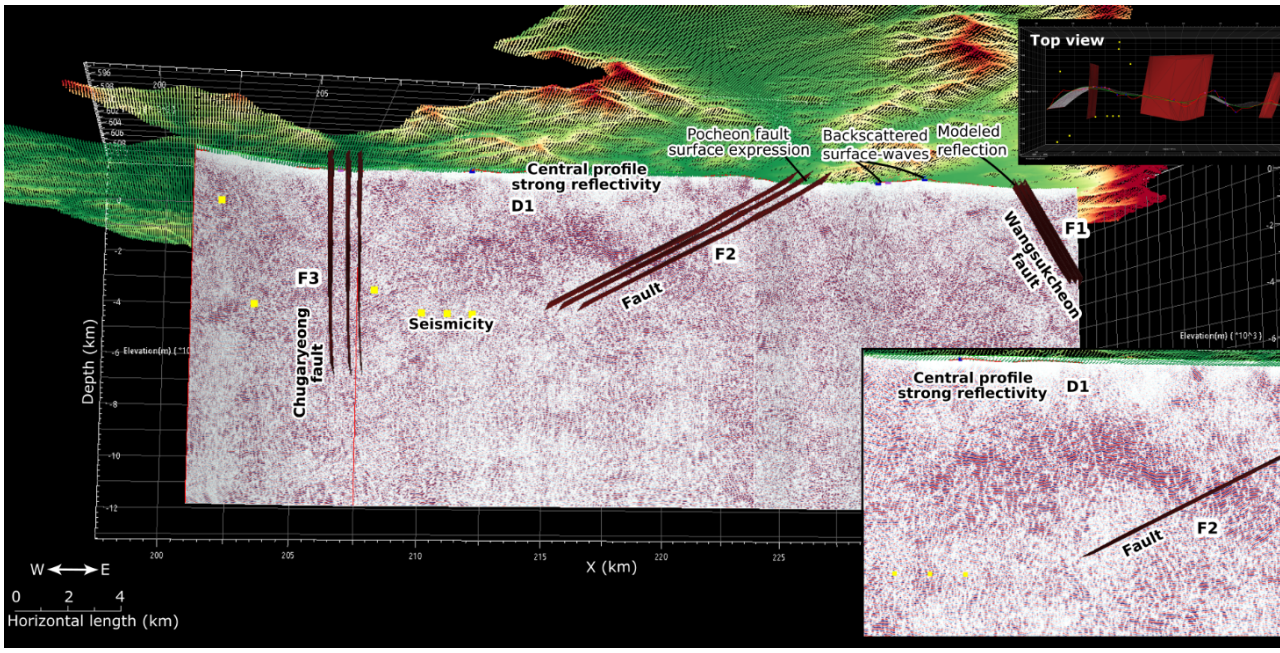


**Figure 8. 3D view of the interpreted fault systems. Migrated stacked section and time-to-depth converted using 6000 m/s velocity from the wireless recorders data. Seismicity is represented with yellow points. Inset shows a portion of the central part of the profile where a fault is interpreted based on an apparent fault-bend fold structure.**

# 7 Conclusions

We have acquired an approximately 40-km long reflection seismic profile intersecting three major fault systems (Chugaryeong, Pocheon and Wangsukcheon faults) in the broader metropolitan area of Seoul in South Korea. The data are consistent with the Chugaryeong fault being a sub-vertical structure below the location where it is geologically mapped. From a seismic viewpoint, surface-waves show strong back scattering from it and it shows no coherent reflectivity. A 30-degree NW dipping zone of reflectivity underlying a dome-shaped reflective package is imaged in the central part of the migrated stacked section and it is interpreted as a fault. A dyke or sill system intersected by the propagating fault has resulted in the fault-bend fold structures (dome-shaped reflectivity). This fault if projected downwards would intersect a series of seismic events at the intersection with the Chugaryeong fault. This further suggests, and confirms a recent speculation, a relation between the two faults concerning the intersection and the seismicity, with the implication that both faults may be active and form splays. If this fault is projected to the surface it will intersect Pocheon fault surface expression and related strong surface wave back scattering, unfortunately

there is no imaging of the near surface geometry of Pocheon fault to confirm or reject this possibility. The Wangsukcheon fault, on the other hand, is found to have a N20E/60E geometry, implying an opposite dip angle from the other two faults. There is no related seismicity associated with the Wangsukcheon fault in the area, which may justify why it has completely different geometry with respect to the two other faults.

*Data availability.* Original data underlying the material presented are available by contacting the corresponding author. However, as the dataset is the subject of other PhD studies, there is a period of 3years embargo on their availability.

*Acknowledgments.* We thank the contributions of many students and post-docs from Yonsei University and Uppsala University, Geopartner and C&H Company. Chiara Colombero and Politecnico di Torino provide access to the surface waves back scattering energy computation code.

*Author contributions.* TKH initiated the project, organized the acquisition and was involved in the discussions of the results and their interpretations. SZ is responsible for the data preparation, for most of the data processing, for the traveltime tomography, for the crossdip analysis, for the interpretations and for the writing of the article. AM led the data acquisition, processed most of the landstreamer data, helped with the overall processing and especially with the writing of the article and the interpretational aspects and discussion. CJ worked in the first part of the data processing highlighting the Wangsukcheon fault reflection and modeling its reflection traveltime. JL helped on the acquisition setting and organization and prepared the basis for the maps. MP worked on the surface-wave back scatterings analysis. BB contributed in the data acquisition and planning. TKH, BB, CJ, JL, MP, SP, DC, BK and JeL contributed to the final preparation of the paper.

*Financial support.* This work was supported by the Korean Meteorological Administration (KMA) Research and Development Program under grant KMI2022-00710, and partly by the Basic Science Research Program of National Research Foundation of Korea (NRF-2017R1A6A1A07015374).

**References**

Ayarza, P., Juhlin, C., Brown, D., Beckholmen, M., Kimbell, G., Pechnig, R., Pevzner, L., Pevzner, R., Ayala, C., Bliznetsov, M., Glushkov, A., and Rybalka, A., 2000. Integrated geological and geophysical studies in the SG4 borehole area, Tagil Volcanic Arc, Middle Urals: Location of seismic reflectors and source of the reflectivity, J. Geophys. Res., vol. 105, no. b9, pages 21,333-21,352.

Bae, H.-K., and Lee, H.-K., 2016. Quaternary activity patterns of the Wangsukcheon Fault in the Pocheon-Namyangju area, Korea, Journal of the Geological Society of Korea, 52(2), 129–147 (in Korean with English abstract).

Beckel, R. and Juhlin, C., 2019. The cross-dip correction as a tool to improve imaging of crooked-line seismic data: a case study from the post-glacial Burtrask fault, Sweden. Solid Earth, 10, 581-598.

Bellefleur, G., Barnes, A., Calvert, A., Hubert, C. and Mareschal, M., 1995. Seismic reflection constraints from Lithoprobe line 29 on the upper crustal structures of the northern Abitibi greenstone belt, Canadian Journal of Earth Sciences, 32, 128–134.

Black, R., Steeples, D., and Miller, R., 1994. Migration of shallow seismic reflection data, Geophysics, V 59, 3, 402-410.

Blonk, B., Herman, G.C., 1994. Inverse scattering of surface waves: A new look at surface Consistency, Geophysics, 59, 963-972, https://doi.org/10.1190/1.1443656.

Brodic, B., Malehmir, A., Juhlin, C., Dynesius, L., Bastani, M. and Palm, H., 2015. Multicomponent broadband digital based seismic landstreamer for near surface applications, J. Appl. Geophys., 123, 227–241.

Choi, S.-J., Chwae, U., Lee, H.-K., Song, Y., and Kang, I.-M., 2012. Review on the Chugaryeong Fault, Journal of Korean Society of Economic and Environmental Geology 45(4), 441–446 (in Korean with English abstract).

Chough, S. K., Kwon, S. -T., Ree, J. -H., and Choi, D. K., 2000. Tectonic and sedimentary evolution of the Korean peninsula: a review and new view, Earth-Science Reviews, 52(1-3), 175–235.

Colombero, C., Comina, C., and Valentina Socco, L., 2019. Imaging near surface sharp lateral variations with surface-wave methods — Part 1: Detection and location, Geophysics, 84(6), EN93–EN111, https://doi.org/10.1190/geo2019-0149.1.

Han, J. W., and Lee, H. K., 2019. Structural behavior and ESR age of the Wangsukcheon Fault developed in Naechon-myeon and Hwahyeon-myeon area, Pocheon, Gyeonggi, Korea. Journal of the Geological Society of Korea. v. 55, no. 4, p. 377-401.

Hong, T.-K., Lee, J., Chi, D., and Park, D., 2017. Seismic velocity changes in the backarc continental crust after the 2011 M w9.0 Tohoku-Oki megathrust earthquake, Geophysical Research Letters, 44, 10997–11003, https://doi.org/10.1002/2017GRL075447.

Hong, T.-K., Lee, J., Park, S., and Kim, W., 2018. Time-advanced occurrence of moderate-size earthquakes in a stable intraplate region after a megathrust earthquake and their seismic properties, Scientific Reports, 8, 13331.

Hong, T.-K., Chung, D., Lee, J., Park, S., Kim, B., and Kim, W., 2021. Earthquake-spawning faults in the Seoul metropolitan area and their seismic implications, Earth and Space Science, 8(7), e2021EA001662. https://doi.org/10.1029/2021EA001662.

Ishiyama, T., Sato, H., Abe, S., Kawasaki, S. and Kato, N., 2016. High-resolution 3D seismic reflection imaging across active faults and its impact on seismic hazard estimation in the Tokyo metropolitan area, Tectonophysics, Volume 689, Pages 79-88, ISSN 0040-1951, https://doi.org/10.1016/j.tecto.2016.01.042.

Kammann, J., Malehmir, A., Brodic, B., Tagliavento, M., Stemmerik, L., Nørmark, E., Lykke-Andersen, H. and Nielsen, L., 2019. Deep onshore reflection seismic imaging of the chalk Group strata using a 45 kg accelerated weight-drop and combined recording systems with dense receiver spacing, Geophysics, 84, B259–B268.

KIGAM (Korea Institute of Geology, Mining & Materials), 2008. Geological report of the Yeoncheon sheet, Korea. Technical Report.

Kim, O. J., 1973. The Stratigraphy and Geologic Structure of the Metamorphic Complex in the Northwestern Area of the Kyonggi Massif, The Korean Society of Economic and Environmental Geology, Volume 6, Issue 4, Pages 201-216 (in Korean with English abstract).

Lee, K., and Yang, W.-S., 2006. Historical seismicity of Korea, B. Seismol. Soc. Am., 96, 846–855.

Lee, Y., Park, S., Kim, J., Kim, H.C. and Koo, M., 2010. Geothermal resource assessment in Korea, Renewable and Sustainable Energy Reviews, 14, 2392-2400.

Malehmir, A., Schmelzbach, C., Bongajum, E., Bellefleur, G., Juhlin, C. and Tryggvason, A., 2009. 3D constraints on a possible deep>2.5 km massive sulphide mineralization from 2D crooked-line seismic reflection data in the Kristineberg mining area, northern Sweden, Tectonophysics, Volume 479, Issues 3–4, Pages 223-240, ISSN 0040-951, https://doi.org/10.1016/j.tecto.2009.08.013.

Malehmir, A., Dahlin, P., Lundberg, E., Juhlin, C., Sjöström, H. and Högdahl, K., 2011. Reflection seismic investigations in the Dannemora area, central Sweden: insights into the geometry of poly-phase deformation zones and magnetite-skarn deposits, J. Geophys. Res., 116, B11307.

Malehmir, A., Zhang, F., Dehgahnnejad, M., Lundberg, E., Döse, C., Friberg, O., Brodic, B., Place, J., Svensson, M. and Möller, H., 2015. Planning of urban underground infrastructure using a broadband seismic landstreamer—Tomography results and uncertainty quantifications from a case study in southwest of Sweden, Geophysics, 80, B177–B192.

Malehmir, A., Andersson, M., Mehta, S., Brodic, B., Munier, R., Place, J., Maries, G., Smith, C., Kamm, J., Bastani, M., Mikko, H. and Lund, B., 2016. Post-glacial reactivation of the Bollnäs fault, central Sweden – a multidisciplinary geophysical investigation, Solid Earth, 7, 509–527.

Malehmir, A., Maries, G., Bäckström, E., Schön, M. and Marsden, P., 2017. Developing cost-effective seismic mineral exploration methods using a landstreamer and a drophammer, Scientific Reports, 7, 10325.

Malehmir, A., Hong, T.-K., Lee, J., Zappalá, S., Brodic, B., Chung, D., Kim, B., Park, S., Lee, J., Kil, D., 2022. Fault intersections control short period intraplate start-stop seismicity in the Korean Peninsula, Tectonophysics, 229387, ISSN 0040-1951, https://doi.org/10.1016/j.tecto.2022.229387.

Nedimović, M. N. and West, G. F., 2003. Crooked-line 2D seismic reflection imaging in crystalline terrains: Part 1, data processing, Geophysics 68: 274-285, https://doi.org/10.1190/1.1543213.

Park, S., Baek, I., and Hong, T.-K., 2020. Six major historical earthquakes in the Seoul metropolitan area during the Joseon dynasty (1392-1910), B. Seismol. Soc. Am., 110 (6), 3037-3049. https://doi.org/10.1785/0120200004.

Rodriguez-Tablante, J., Tryggvason, A., Malehmir, A., Juhlin, C. and Palm, H., 2007. Cross-profile acquisition and cross-dip analysis for extracting 3D information from 2D surveys, a case study from the western Skellefte District, northern Sweden, J. Appl. Geophys., Volume 63, Issue 1, Pages 1-12, ISSN 0926-9851, https://doi.org/10.1016/j.jappgeo.2007.03.001.

Rosenblueth, E. and Ordaz, M.., 1990. Maximum Earthquake Magnitude at Fault, J. Eng. Mech.-Asce, 116, 10.1061/(ASCE)0733-9399(1990)116:1(204).

Sato, H., Ito, K., Abe, S., Kato, N., Iwasaki, T., Hirata, N., Ikawa, T. and Kawanaka T., 2009. Deep seismic reflection profiling across active reverse faults in the Kinki Triangle, central Japan, Tectonophysics, Volume 472, Issues 1–4, Pages 86-94, ISSN 0040-1951, https://doi.org/10.1016/j.tecto.2008.06.014.

Singh, S. K., Bazan, E. and Esteva, L., 1980: Expected Earthquake Magnitude from a Fault, Bull. seism. Soc. Am., 70. 10.1785/BSSA0700030903.Suppe, J. and Medwedeff, D., 1990. Geometry and kinematics of fault-propagation folding, Eclogae Geologicae Helvetiae, 83, 409-454.

Wells, D. and Coppersmith, K., 1994. New Empirical Relationships among Magnitude, Rupture Length, Rupture Width, Rupture Area, and Surface Displacement, B. Seismol. Soc. Am. ,84, 974-1002.

Yu, H., Guo, B., Hanafy, S., Schuster, G.T., Lin, F.-C., 2014. Direct detection of near-surface faults by migration of back-scattered surface waves, SEG Technical Program Expanded Abstracts, 2135-2139.

Zerwer, A., Polak, M.A. and Santamarina J.C., 2005. Detection of Surface Breaking Cracks in Concrete Members Using Rayleigh Waves, J. Environ. Eng. Geoph., 10(3):295-306. doi: 10.2113/JEEG10.3.295.

Zoback, M.D., Hickman, S., and Ellsworth, W.L., 2010. Scientific drilling into the San Andreas Fault. Eos, Trans, AGU, 91(22), 197–204, doi:10.1029/2010EO220001.